Open Access Library Journal
2022, Volume 9, e9497
ISSN Online: 2333-9721
ISSN Print: 2333-9705

Comparative Study between Different Macroscopic Approximations for Cold Plasma Modeling

Moustapha Ouali*, Najlae Seddaoui, Youssef Lagmich

Laboratory of Sciences and Advanced Technologies Polydisciplinary, Faculty of Larache, Abdelmalek Essaâdi University, Larache, Morocco
Email: *moustaphaouaali@gmail.com

How to cite this paper: Ouali, M., Seddaoui, N. and Lagmich, Y. (2022) Moustapha Ouali, Najlae Seddaoui, Youssef Lagmich. *Open Access Library Journal*, **9**: e9497.
https://doi.org/10.4236/oalib.1109497

Received: October 28, 2022
Accepted: November 26, 2022
Published: November 29, 2022

Abstract

Several methods can be used to model the plasma, especially to solve the Maxwell-Boltzmann equation. In fact, the plasma is treated as a charged fluid in order to have an alternative solution for the resolution of the Maxwell-Boltzmann equation. This macroscopic model according to the complexity admits two approximations called Local Field Approximation and Local Energy Approximation. Consequently, the major objective of this article is to realize a comparative study between these two macroscopic approximations while highlighting the use of each one. A two-dimensional model of the non-equilibrium discharge is realized, with the presence of a dielectric barrier while using the COMSOL Multiphysics program. The results of the numerical simulations showed a remarkable effect in making the function that relates the average electronic energy with the reduced field in the case of a Local Field Approximation well specified. From the study realized, it is shown that when the frequency is increased, the results obtained by the Local Field Approximation diverge at high frequency, it is also shown that this leads to a Townsend transition to the streamer discharge mode. Moreover, the results obtained by the Local Energy Approximation are consistent with those existing in the literature.

Subject Areas

Plasma Physics

Keywords

Dielectric Barrier Discharge, Cold Plasma, Local Field, Local Energy, Atmospheric Pressure

*Corresponding author.

1. Introduction

Cold plasma technology has attracted the attention of several researchers due to its importance in many fields such as medicine, the industry as well as agriculture and biotechnology, and others [1] [2] [3] [4]. Due to its important chemical and physical properties, plasma is a micro discharge created by an electric field between two electrodes that are separated by a dielectric [3]; if a very high current is applied to the electrodes, the dielectric's function is to accumulate charges on its surface to prevent the formation of an electric arc by weakening the electric field between the two electrodes [5] [6]. This process is called a dielectric barrier discharge. This discharge has some interesting characteristics including the excitation frequency being around kHz, the inter-electrode distance being around a few millimeters, at least one or both electrodes being covered by a dielectric and the applied voltage being around a few kV. To better understand the influence of these parameters, a simulation of a two-dimensional model is required.

In addition, there are several research works whose objective is to carry out a parametric study of the influence of pressure, applied voltage, distance between the two metal electrodes, frequency or gas [3] [7] [8]. However, before carrying out these studies, it is necessary to choose the physical model, and in this sense, our work focuses on how to choose the appropriate approximation to model the discharge in question, as well as the advantages and disadvantages of each.

2. Modeling of a Dielectric Barrier Discharge

A two-dimensional model of a dielectric barrier discharge is used in this work, with a single dielectric, in order to better understand the evolution of different parameters that characterize this type of discharge. Simulations are performed for different pressures ranging from 60 Torr to 760 Torr equivalent of 1 atm, a discharge inter-electrode gap equal to 3 mm, and a 1 kV sinusoidal applied voltage at various frequencies between 200 Hz to 50 Hz (**Figure 1**).

Figure 1. Simulation model.

The macroscopic model allows treating the plasma as a charged fluid. The fluid model is more efficient in solving the resulting equations since it describes the plasma in terms of macroscopic parameters based on a specific form of the distribution function while taking into consideration the velocity moments of

the Boltzmann equation, it is also easy to couple the electron dynamics to the electric field. However, we end up with a set of coupled differential equations that can be solved using numerical methods. Depending on the desired application, this model admits two approximations called "Local Field Approximation" and "Local Energy Approximation", which are characterized by physical quantities such as the density, the average velocity and the average energy of particles [7] [8] [9].

2.1. Local Energy Approximation

In order to solve the Boltzmann equation, a system composed of three fluid equations called the moment of Boltzmann equation will be solved to expose the physical characteristics in terms of mean quantities such as mean density, energy and velocity to better understand the behavior of the plasma based on the dielectric barrier discharge [10]. This numerical model of the dielectric barrier discharge allows solving the second moment of the Boltzmann equation, which is the conservation equation of mean electronic energy, in a self-consistent way with the conservation equation of momentum and Poisson and the continuity equations. Furthermore, this model allows using the mean electronic energy of the particles to parameterize the transport coefficients, the mean collision frequencies and the electronic energy distribution functions. This is the most demanding option in numerical terms, to find the average electronic energy because of the strong link between the mean electronic energy and the electric fields [7] [10] [11] [12].

$$\frac{\partial n_k}{\partial t} + \nabla\left(\Gamma_k\right) = S_k \tag{1}$$

$$\frac{\partial\left(n_e m_e u_e\right)}{\partial t} + \nabla \cdot n_e m_e u_e = -\left(\nabla \cdot p_e\right) + q n_e E - n_e m_e u_e \nu_m \tag{2}$$

The continuity Equation (1) can be used to represent the variation rates of the density of charged species, where n_k is the volume mass, S_k is the source term that depends on the ionization and Γ_k is the k-particle flux ($k = e, i$ refers to electrons and positive ions).

The rate of variation of the electron momentum is described by Equation (2): where m_e is the electron mass, p_e is the electron pressure tensor, u_e is the electron drift velocity, E is the electric field, q is the electron charge and ν_m is the momentum transfer frequency.

To find the flux term in Equation (2), a different simplification known as the drift-diffusion approximation is employed in place of the explicit solution of the first moment of the Boltzmann equation. The ionization and attachment frequencies and the angular frequency are much lower than the angular momentum transfer frequency, the first term on the left side of Equation (2) can be neglected alternatively, and the second term in Equation (2) can be ignored, by assuming that the electron drift velocity is less than the thermal velocity. In the case of a Maxwellian distribution, the pressure term, p_e, can be replaced by the Equation (3), where I is the identity matrix and T_e is the electron temperature.

$$p_e = n_e k_B T_e I \tag{3}$$

Finally, the charged particle flux is given by Equation (4) with μ_k, D_k and E are the mobility of charged species, the diffusion coefficient and the electric field respectively

$$\Gamma_k = n_k u_k = B \cdot \left(n_k \mu_k E - \nabla n_k D_k \right) \tag{4}$$

$$B = \begin{cases} -1 & \text{for electrons} \\ +1 & \text{for ions} \end{cases}$$

The energy conservation Equation (5) is exploited to establish the final expression for the electron energy density, including the drift-diffusion approximation. With ε the mean electron energy, S_ε the energy of the electrons lost by collisions, Γ_e the mean electron flux energy, μ_ε the electron mobility and D_ε the electron flux diffusion coefficient.

$$\frac{\partial \left(n_e \varepsilon \right)}{\partial t} + \nabla \left(\Gamma_\varepsilon \right) + E \cdot \Gamma_e = S_\varepsilon \tag{5}$$

With:

$$\Gamma_\varepsilon = -n_\varepsilon \mu_\varepsilon E - \nabla_\varepsilon D_\varepsilon$$

By applying the Maxwellian electron energy distribution function, the energy diffusivity Equation (6), energy mobility Equation (7), and electron diffusivity Equation (8) are determined from the electron mobility.

$$D_e = \mu_e T_e \tag{6}$$

$$\mu_\varepsilon = \frac{5}{3} \mu_e \tag{7}$$

$$D_\varepsilon = \mu_\varepsilon T_e \tag{8}$$

The following boundary condition results from the concentration of charges on the dielectric surface, where $\boldsymbol{\varepsilon}_1$ and $\boldsymbol{\varepsilon}_1$ are the gas's and the dielectric's respective relative permittivities.

$$n \cdot \left(D_1 - D_2 \right) = \rho \tag{9}$$

$$n \cdot \left(E_1 \varepsilon_1 - E_2 \varepsilon_2 \right) = \rho \tag{10}$$

The fluid equations, where V is the electrostatic potential, ε_0 is the space permittivity and q is the electron charge, are used to determine the electric field using Poisson's Equation (11).

$$\Delta V = \frac{q}{\varepsilon_0} \left(n_e - n_i \right) \tag{11}$$

$$E = -\nabla V$$

2.2. Local Field Approximation

This approximation is based on the solution of the two Boltzmann transport equations, the continuity equation and the momentum conservation equation, which are coupled to the Poisson equation, without needing to solve the energy density

equation, since this approximation consists of supposing that the distribution function of the charged particles at a given time and position is the same as that obtained for a uniform electric field, which corresponds to the value of the field existing at that time and position, and this considerably reduces the complexity of the numerical problem. However, when the Local Field Approximation is used; a function that relates the mean electron energy and the reduced electric field must be provided (Equation (12)), or it is possible to fix the mean electron energy at its initial value [7] [9] [11] [13].

$$\varepsilon = F\left(\frac{E}{N}\right) \tag{12}$$

In this case, this approximation is conditioned by a balance between the electron energy gain rate and the energy loss rate; *i.e.* the energy gained by the electrons due to the electric field is exactly compensated by the losses due to collisions. This is equivalent to an energy equation composed of only the electric force term and the collisional energy loss term. When this condition is satisfied, the electrons are in local equilibrium with the electric field, and the mean properties of the electrons can be expressed as a function of the reduced electric field [14] [15] [16].

3. Results and Discussion

The results of the simulations carried out in this work are based on the two approximations that of the local energy and the local field in order to compare them. The simulations were executed for different values of pressures varying from 60 Torr to 760 Torr, a band of frequencies varying between 200 Hz and 10 kHz, space of discharge between the electrodes equal to 3 millimeters with a voltage applied of 1 kV, a temperature of 300 K, the gas used in these studies is the helium, a coefficient of secondary emission of 0.01.

3.1. Low-Pressure Discharge

In a low-pressure discharge, the densities of neutral particles and charged species are weak, which minimizes the number of collisions between the particles, and makes the mean free path quite important. This generates a weak or negligible electric field. This type of discharge is described by the "Townsend mechanism". Figure 2 shows the temporal evolution of the electrical characteristics calculated during two cycles of applied voltage at a low pressure of 60 Torr, a frequency of the applied voltage equal to 200 Hz and a discharge distance between the electrodes of 3 mm. The results obtained by the two approximations, local energy (a) and local field (b), show that the current and voltage waveforms present several peaks per half cycle of applied voltage. The breakdown voltage equals 488V for LEA while it is less than 100 V for LFA. Indeed, each micro-discharge induces a current pulse with an average duration of a few tens of microseconds.

Figure 3 and Figure 4 present the results of simulations obtained for frequencies of the applied voltage of 1 kHz and 10 kHz respectively, (a) by the Local

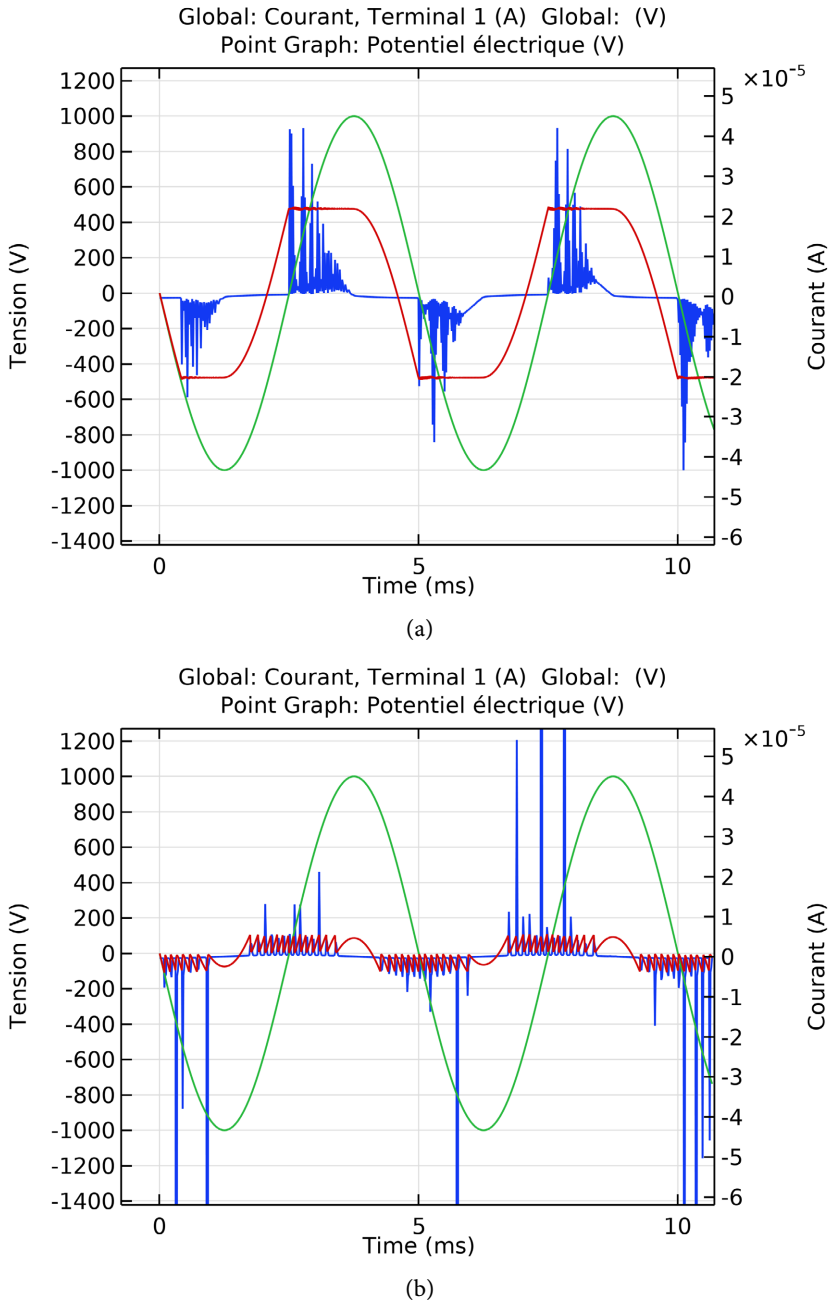

Figure 2. Calculated discharge current profile (blue) and gas voltage (red) at an applied voltage of 1 kV (green) at a low frequency of 200 Hz, $d = 3$ mm and $P = 60$ Torr.

Energy Approximation (LEA) and (b) by the Local Field Approximation (LFA). According to the results, the increase of the frequency leads to a decrease of the number of current peaks at each half-cycle of the applied voltage, in fact, this increase allows the passage from the filamentary regime to the homogeneous regime. With the LEA, more the frequency increases, more the multi-peaks of the current and of the breakdown voltage are reduced to two peaks for the first half-cycle and three peaks for the rest. Moreover, the current intensity increases from 0.15 mA to 5 mA, and the breakdown voltage amplitude reaches 600 V.

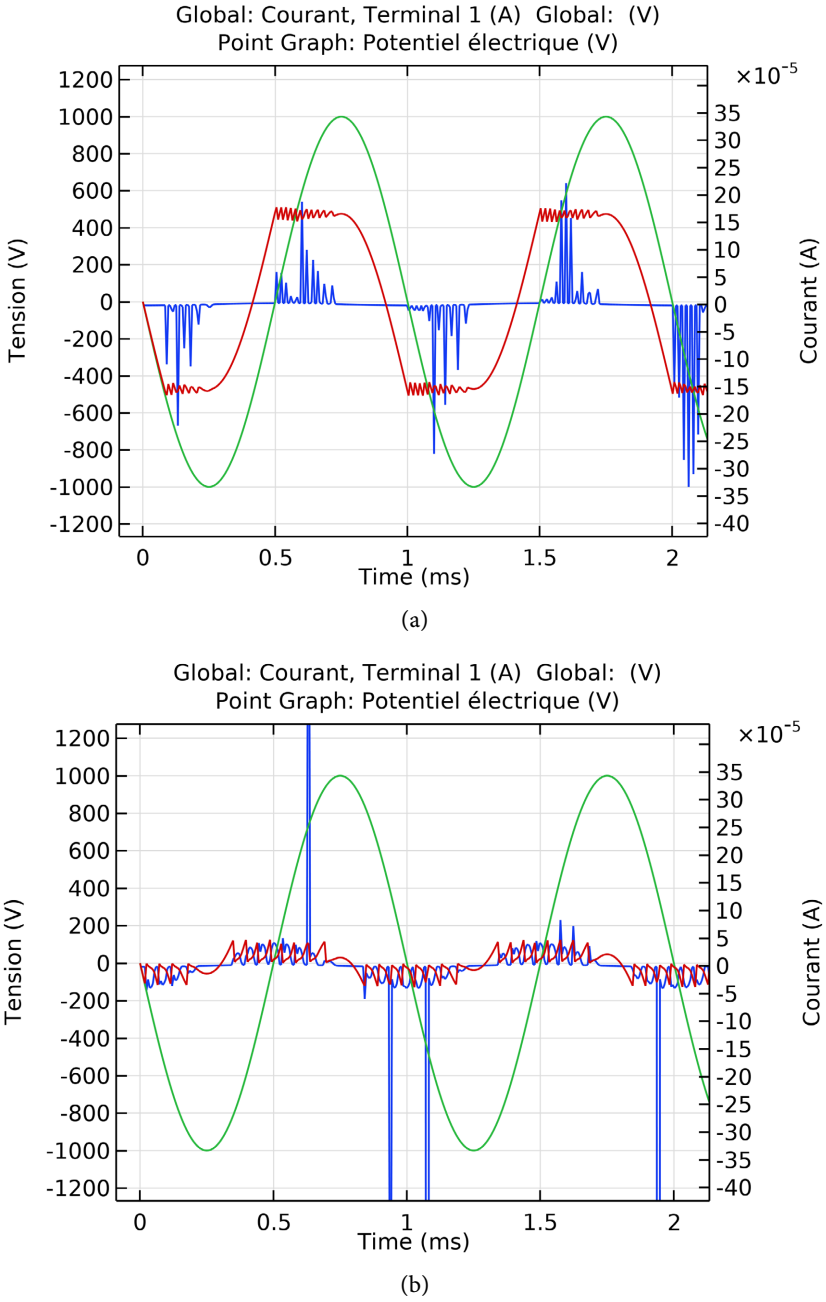

Figure 3. Calculated discharge current profile (blue) and gas voltage (red) at an applied voltage of 1 kV (green) at a low frequency of 1 kHz, $d = 3$ mm and $P = 60$ Torr.

Regarding LFA with average electronic energy fixed at its initial value, with the increase of the frequency of the applied voltage, the current peaks disappear for the first half-cycle and decrease for the rest, even for the breakdown voltage the number of peaks decreases during time. However, when increasing the frequency to 10 kHz the results diverge.

We conclude that the simulation based on the Local Energy Approximation permits to have results whatever the frequency of the applied voltage, but the Local Field Approximation diverges at high frequencies.

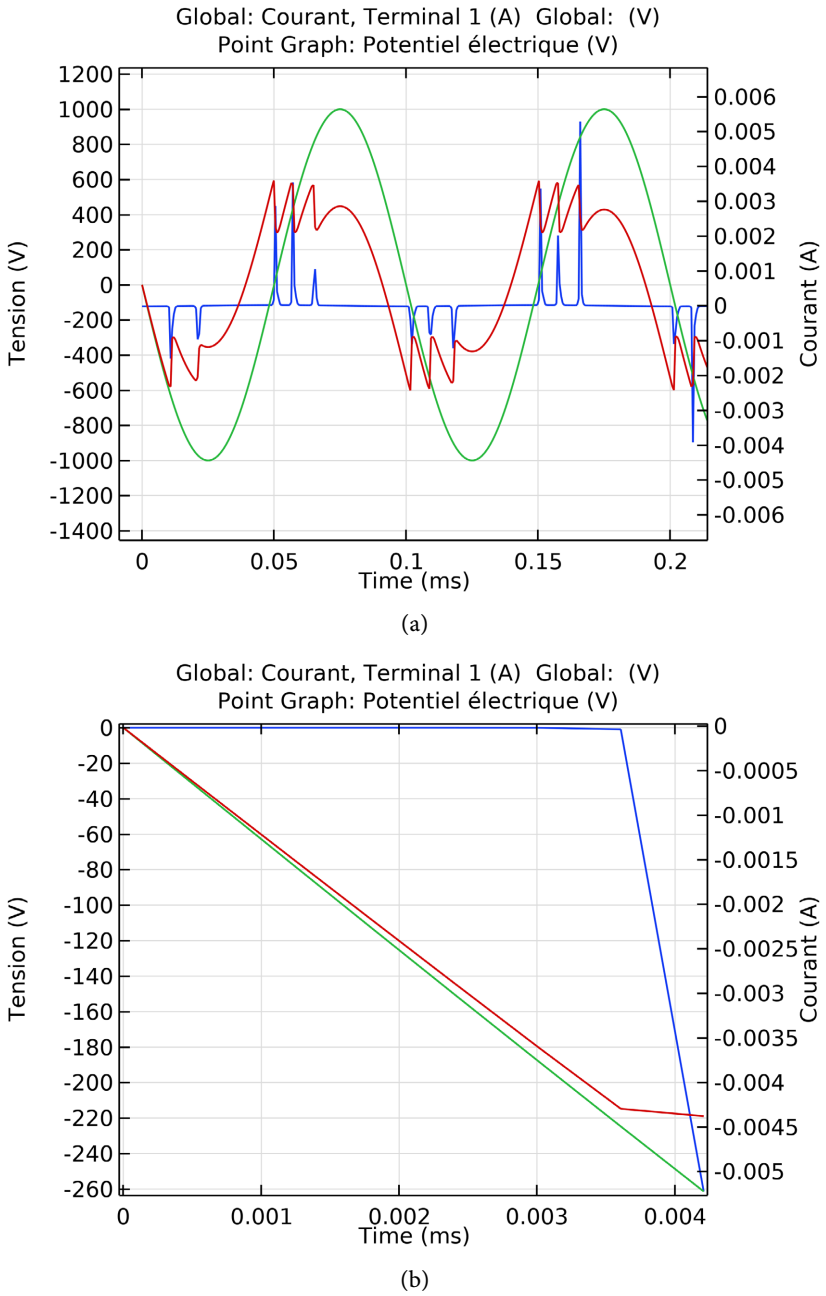

Figure 4. Calculated discharge current profile (blue) and gas voltage (red) at an applied voltage of 1 kV (green) at a low frequency of 10 kHz, $d = 3$ mm and $P = 60$ Torr.

3.2. High-Pressure Discharge

With more interactions between particles and a smaller mean free path, the high-pressure discharge produces larger species densities. Because of this, the electric field is significant and has a big impact on how the gas breaks down. This is known as the "streamer mechanism". **Figure 5** presents the electrical characteristics calculated when applying two cycles of the voltage at atmospheric pressure (760 torr). The simulation results with an inter-electrode distance of 3mm diverge with the Local Field Approximation. For this reason, the rest of the

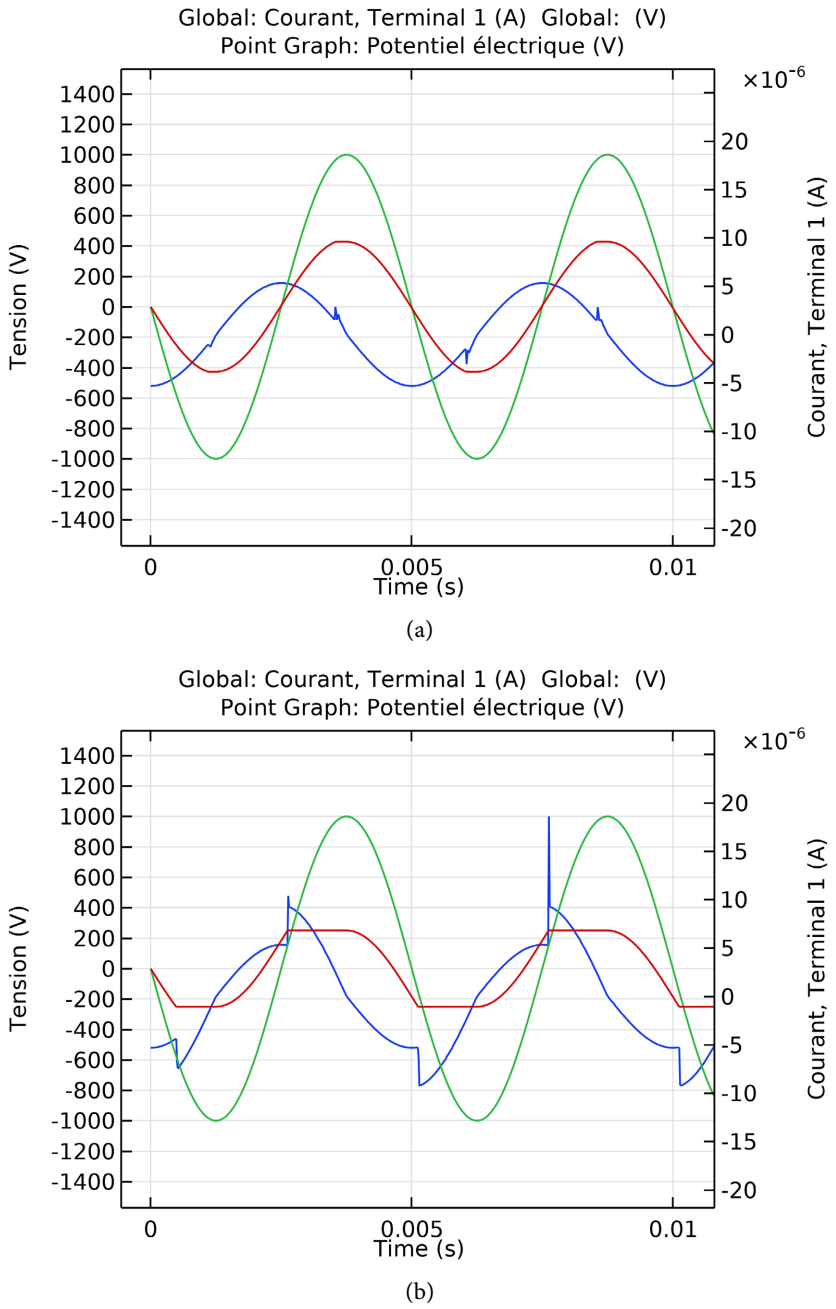

Figure 5. Calculated discharge current profile (blue) and gas voltage (red) at an applied voltage of 1 kV (green) at a low frequency of 200 Hz, $d = 0.1$ mm and $P = 760$ Torr.

simulations are done with a discharge distance equal to 0.1 mm. per each half cycle of applied voltage, the electric current obtained by the two approximations admits a single peak.

Figure 5 and **Figure 6** show the results of simulations with an applied voltage frequency of 200 Hz and 1 kHz, respectively. These results demonstrate that as the applied voltage frequency rises, the intensity of the discharge current produced by the two approximations of local energy (a) and local field (b) also rises. whereas the breakdown voltage keeps the same shape with the same amplitude.

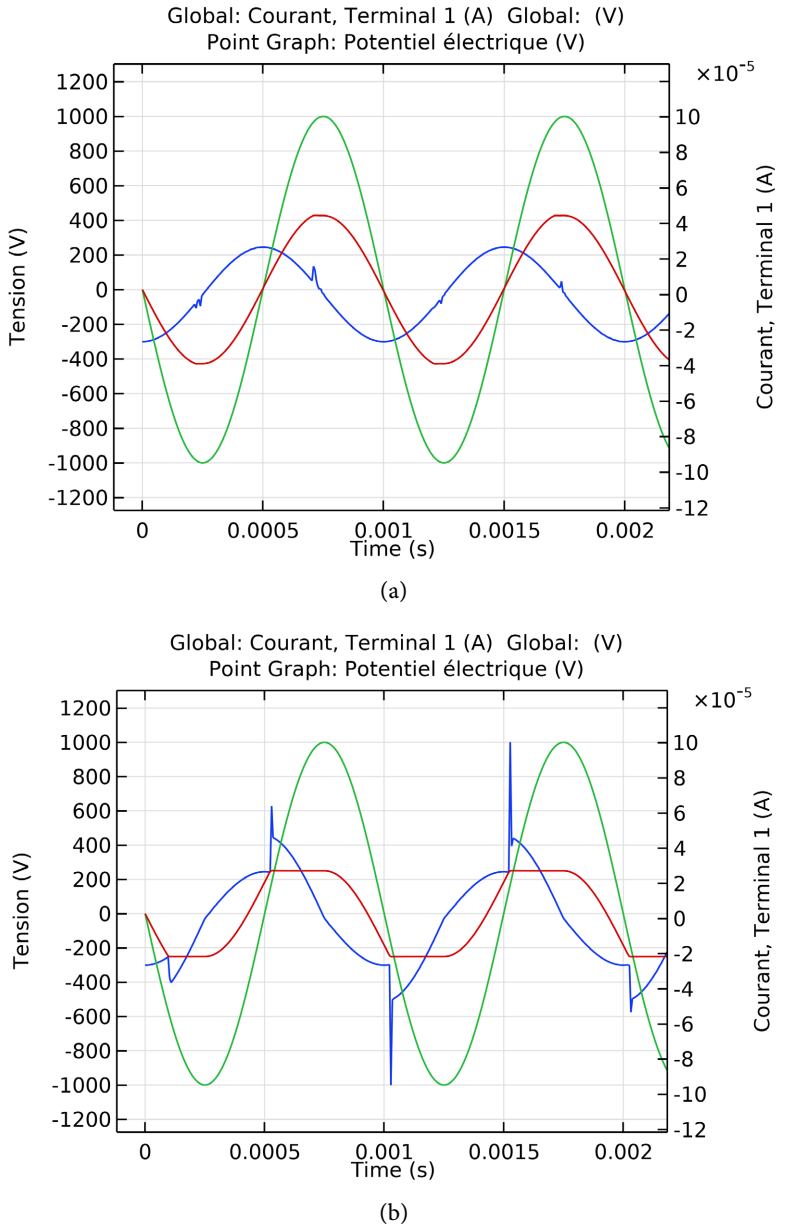

Figure 6. Calculated discharge current profile (blue) and gas voltage (red) at an applied voltage of 1 kV (green) at a low frequency of 1 kHz, $d = 0.1$ mm and $P = 760$ Torr.

Generally, the triggering of a discharge occurs when its voltage exceeds the breakdown voltage imposed by the gas (here helium), and ends when its voltage becomes lower than the rupture voltage. The peaks are exposed due to the accumulation of several discharges in the same voltage cycle as shown in **Figure 7**, However, the voltage goes to the rupture voltage. As the voltage increases, the applied voltage also increases with each cycle due to the surcharge at the barrier dielectric. Therefore, the previous treatment improves the gap and involves several peaks in a single cycle. On the other hand, the voltage cycle time interval also plays an important role at higher frequencies and exactly when the time between cycles is insufficient so the discharge does not show multiple breakdowns.

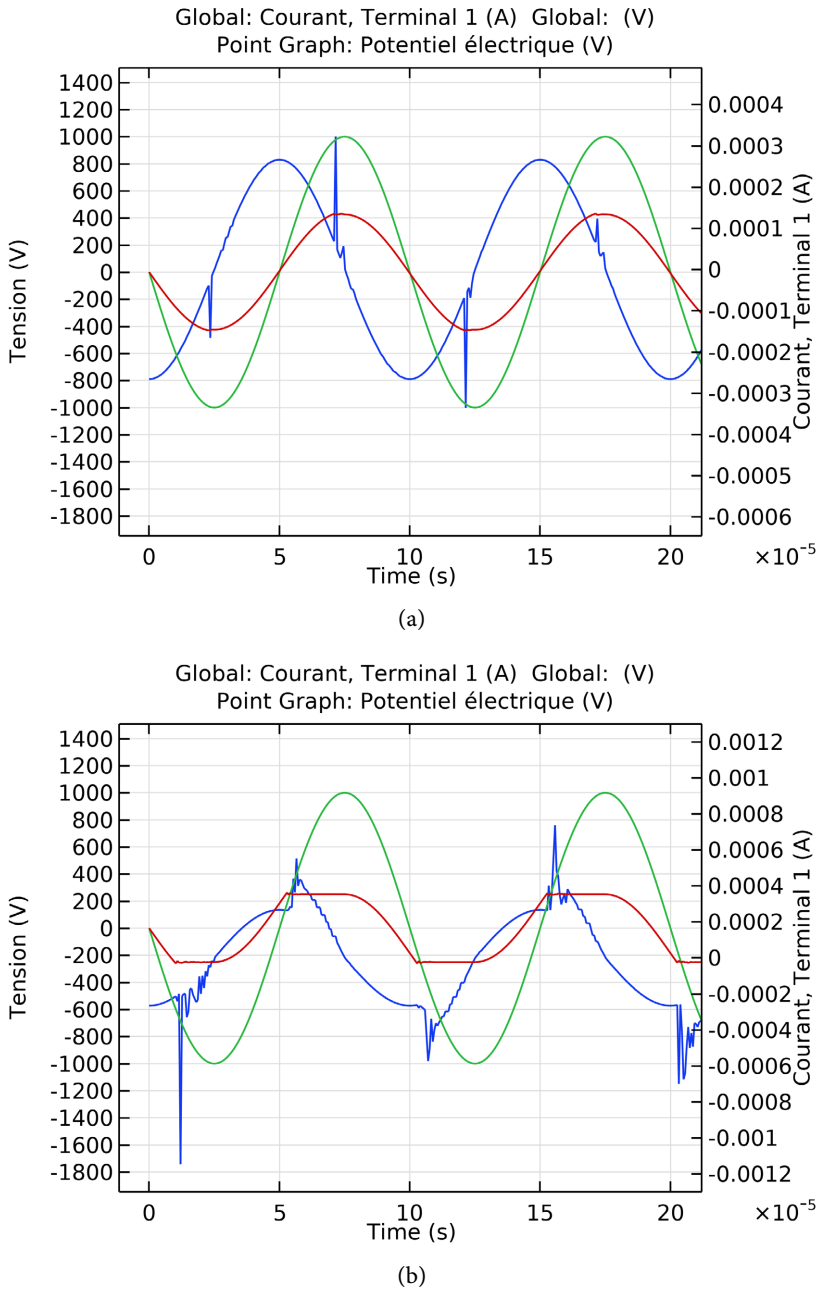

Figure 7. Calculated discharge current profile (blue) and gas voltage (red) at an applied voltage of 1 kV (green) at a low frequency of 10 kHz, $d = 0.1$ mm and $P = 760$ Torr.

4. Conclusions

A numerical analysis of a dielectric barrier discharge is carried out using a 2D fluid model in this work. The principal objective of this work is to compare the two macroscopic approximations, the local energy and the local field, as well as the influence of the applied voltage frequency and pressure on the electrical characteristics of this discharge. The results of the simulations obtained show how important it is to take the energy equation into consideration. However, the choice between the two approximations depends on several parameters such as the cal-

culation time, the precision of the desired results and many others.

Additionally, it has been discovered that when the applied voltage frequency rises, the maximum amplitude of the discharge current likewise rises. This increase also leads to a decrease in the number of peaks per half cycle of applied voltage; thus, leading to a transition from the filamentary to the homogeneous regime. Furthermore, the inability of the Local Field Approximation to produce results for high frequencies can be explained by the loss of the critical condition for its performance during the simulation, which is local equilibrium. The electronic energy gain rate caused by the electric field is not in balance with the energy loss rate.

Conflicts of Interest

The authors declare no conflicts of interest.

References

[1] Starek, A., *et al.* (2019) Evaluation of Selected Microbial and Physicochemical Parameters of Fresh Tomato Juice after Cold Atmospheric Pressure Plasma Treatment during Refrigerated Storage. *Scientific Reports*, **9**, Article No. 8407. https://doi.org/10.1038/s41598-019-44946-1

[2] Gidon, D., Abbas, H.S., Bonzanini, A.D., Graves, D.B., Mohammadpour Velni, J. and Mesbah, A. (2020) Data-Driven LPV Model Predictive Control of a Cold Atmospheric Plasma Jet for Biomaterials Processing. *Control Engineering Practice*, **109**, Article ID: 104725. https://doi.org/10.1016/j.conengprac.2021.104725

[3] Seddaoui, N., Ouali, M. and Lagmich, Y. (2022) Atmospheric Pressure Plasma Jet Based on the Dielectric Barrier Discharge. *ITM Web of Conferences*, **48**, Article No. 02008. https://doi.org/10.1051/itmconf/20224802008

[4] Barekzi, N. and Laroussi, M. (2013) Effects of Low Temperature Plasmas on Cancer Cells. *Plasma Processes and Polymers*, **10**, 1039-1050. https://doi.org/10.1002/ppap.201300083

[5] Brandt, S., Klute, F.D., Schütz, A. and Franzke, J. (2017) Dielectric Barrier Discharges Applied for Soft Ionization and Their Mechanism. *Analytica Chimica Acta*, **951**, 16-31. https://doi.org/10.1016/j.aca.2016.10.037

[6] Klute, F.D., Schütz, A., Brandt, S., Burhenn, S., Vogel, P. and Franzke, J. (2018) Characterization of Dielectric Barrier Discharges for Analytical Chemistry. *Journal of Physics D: Applied Physics*, **51**, Article ID: 314003. https://doi.org/10.1088/1361-6463/aace24

[7] Turner, M.M. (2013) Numerical Effects on Energy Distribution Functions in Particle-in-Cell Simulations with Monte Carlo Collisions: Choosing Numerical Parameters. *Plasma Science and Technology*, **22**, Article ID: 055001. https://doi.org/10.1088/0963-0252/22/5/055001

[8] Hu, W., Liu, Q. and Zhang, C. (2020) Study on the Differences between Atmospheric Pressure Dielectric Barrier Discharge in Oxygen and Nitrogen Gas. 5*th Asia Conference on Power and Electrical Engineering* (*ACPEE*), Chengdu, 4-7 June 2020, 1945-1949. https://doi.org/10.1109/ACPEE48638.2020.9136341

[9] Li, C., Brok, W.J.M., Ebert, U. and Van Der Mullen, J.J.A.M. (2007) Deviations from the Local Field Approximation in Negative Streamer Heads. *Journal of Applied Physics*, **101**, Article ID: 123305. https://doi.org/10.1063/1.2748673

[10] Gadkari, S. and Gu, S. (2017) Numerical Investigation of Co-Axial DBD: Influence of Relative Permittivity of the Dielectric Barrier, Applied Voltage Amplitude, and Frequency. *Physics of Plasmas*, **24**, Article ID: 053517. https://doi.org/10.1063/1.4982657

[11] Van Laer, K. and Bogaerts, A. (2015) Fluid Modelling of a Packed Bed Dielectric Barrier Discharge Plasma Reactor. *Plasma Sources Science and Technology*, **25**, Article ID: 015002. https://doi.org/10.1088/0963-0252/25/1/015002

[12] Liu, L., Mihailova, D.B., Van Dijk, J. and Ten Thije Boonkkamp, J.H.M. (2014) Efficient Simulation of Drift-Diffusive Discharges: Application of the "Complete Flux Scheme". *Plasma Sources Science and Technology*, **23**, Article ID: 015023. https://doi.org/10.1088/0963-0252/23/1/015023

[13] Wang, Z. and Zhuang, P. (2021) Spin Polarization Induced by Inhomogeneous Dynamical Condensate. 1-11.

[14] Sohbatzadeh, F. and Soltani, H. (2018) Time-Dependent One-Dimensional Simulation of Atmospheric Dielectric Barrier Discharge in $N_2/O_2/H_2O$ Using COMSOL Multiphysics. *Journal of Theoretical and Applied Physics*, **12**, 53-63. https://doi.org/10.1007/s40094-018-0281-4

[15] Liu, N. and Pasko, V.P. (2004) Effects of Photoionization on Propagation and Branching of Positive and Negative Streamers in Sprites. *Journal of Geophysical Research: Space Physics*, **109**, A04301. https://doi.org/10.1029/2003JA010064

[16] You, Q., Mo, N., Liu, X., Luo, H. and Shi, Z. (2020) Experiments on Helium Breakdown at High Pressure and Temperature in Uniform Field and Its Simulation Using COMSOL Multiphysics and FD-FCT. *Annals of Nuclear Energy*, **141**, Article ID: 107351. https://doi.org/10.1016/j.anucene.2020.107351